A tracking motion approach for a piezotube actuator in a disk drive subject to disk deformation and disturbance

2007 Smart Mater. Struct. 16 1542

(http://iopscience.iop.org/0964-1726/16/5/006)

IOP Publishing Smart Materials and Structures
Smart Mater. Struct. **16** (2007) 1542–1548 doi:10.1088/0964-1726/16/5/006

A tracking motion approach for a piezotube actuator in a disk drive subject to disk deformation and disturbance

C S Chang, T S Liu[1] and Y C Tang

Department of Mechanical Engineering, National Chiao Tung University, Hsinchu 30010, Taiwan, Republic of China

E-mail: tsliu@mail.nctu.edu.tw

Received 3 April 2007, in final form 26 June 2007
Published 27 July 2007
Online at stacks.iop.org/SMS/16/1542

Abstract
This study investigates the disk drive dynamics when a disk surface deforms and a disturbance force is exerted on a pickup head in near-field optical disk drives. Serving as an actuator, a piezotube is connected to the suspension of the pickup head. A model is constructed to investigate the pickup head dynamics. Equations of motion for focusing and track-following are derived in the presence of disk surface deformation and the disturbance force on the pickup head. A proportional and derivative control method is carried out in numerical examples. There exists a critical proportional gain that influences the number of resonances in the frequency spectra. Numerical results show that there is only one resonance or none in the frequency spectra when the proportional gain is larger than the critical proportional gain. Hence, the tracking error ratio becomes smaller than one within a wide frequency range, if few resonances appear in the frequency spectra.

(Some figures in this article are in colour only in the electronic version)

1. Introduction

In recent years, several types of optical data storage systems based on near-field optics have been proposed for next-generation ultra-high-density storage [1–4]. A readout method using a near-field optical head, which consists of an aspheric lens and a solid immersion lens (SIL), has been proposed to read out 30 Gb (gigabytes) or more on a 12 cm disk. As depicted in figure 1, it is necessary to maintain an air gap between the SIL bottom surface and the disk surface in a near-field position so that an evanescent wave is detectable. It is also necessary to follow a track steadily on disks of a few tens of nanometer track pitch. Hence, the near-field optical disk drive (NFODD) adopts a flying pickup head structure to maintain the air gap and uses a voice coil motor to follow the track. However, since optical disks are generally made of a plastic-based material, the disk vibration amplitude will be severe. Therefore, in the near field the passive air bearing and voice coil motor hardly meet both the focusing and track-following requirements.

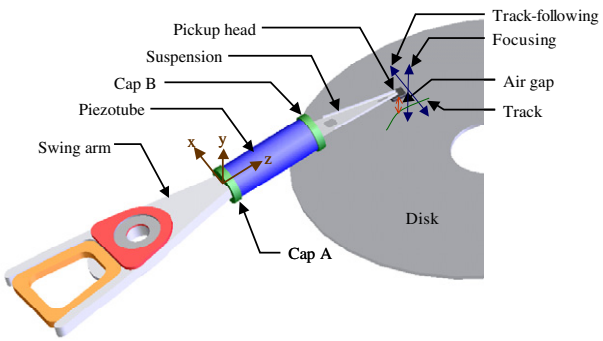

Figure 1. Pickup head with a piezotube actuator in the near-field disk drive.

Wu and Liu [5] designed a PZT bender actuator in an NFODD to control the air gap. In this study, a piezotube actuator is used to meet both air gap and track-following requirements. Piezotubes have been used in near-field microscopy such as in a scanning tunneling microscope

[1] Author to whom any correspondence should be addressed.

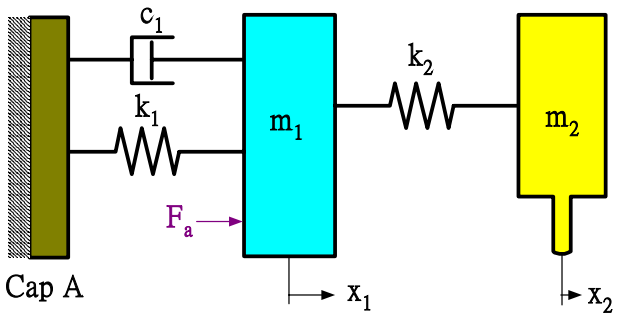

Figure 2. Discrete model of a pickup head with a piezotube actuator during track-following.

(STM) [6] and scanning probe microscope (SPM) [7] to carry out scanning motion. The tube actuator offers a compact design, motion in three degrees of freedom, and low-cost construction. Therefore, this study uses a piezotube that connects to a suspension in the pickup head of an NFODD.

The effects of the disk surface deformation and disturbance force on pickup head dynamics are crucial for reducing tracking error in NFODD. The effect of air bearings on slider dynamics was analyzed by Tanaka *et al* [8]. Kim *et al* [9] studied disk vibration and rotating airflow in magneto-optical disk drives. Honchi *et al* [10] presented a contact model and investigated the slider vibration during slider–disk contact. Kim *et al* [11] designed a small optical flying head and investigated its flying stability and disk durability. Hong *et al* [12] investigated the dynamics of the head–disk assembly for small form factor optical disk drives. Kim *et al* [13] presented the flying stability of optical flying heads during loading/unloading. Since the proportional and derivative (PD) control method has advantages of fast response and low cost, this study investigates the performances of focusing and track-following with PD control in the presence of disk surface deformation and disturbance force for pickup heads endowed with a piezotube actuator.

2. Dynamic model

A pickup head with a piezotube actuator in a near-field disk drive is shown in figure 1. The head has to move along the x-axis for following data tracks on a disk, which is called track-following motion. It also has to maintain along the y-axis an air gap between the pickup head and disk, which is called focusing motion. During reading/writing, the pickup head has to track a desired data track, which constitutes tracking motion. Furthermore, to match the lens focal length, the pickup head still cannot read/write data unless it can follow the vibratory deformation of a rotating optical disk and hence fly up and down along the y-axis. The flying height varies by tracking the disk deformation to maintain a stable distance for focusing. Based on the tracking motion approach, this study investigates both track-following and focusing motions in the frequency spectrum.

Figure 2 shows a lumped model consisting of two masses, two springs and one damper to account for the dynamics among the piezotube, suspension, and pickup head. Figure 3 depicts a piezotube actuator excited in the x-direction by

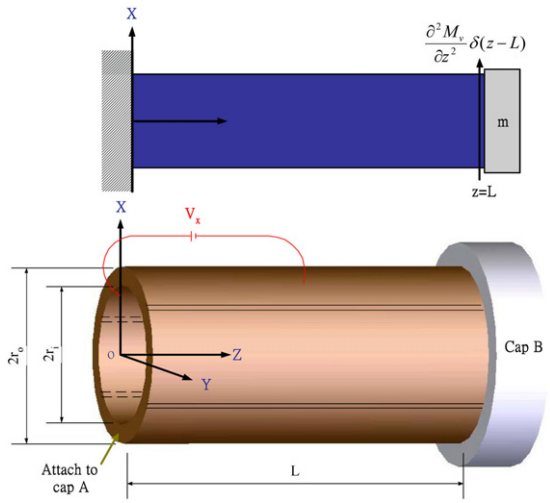

Figure 3. Schematic of the piezotube actuator excited in the lateral direction.

applying a voltage to one of outer electrodes. The equation of motion in lateral dynamics is written as [7]

$$\rho A\frac{\partial^2 w}{\partial t^2}+c_{\mathrm{w}}\frac{\partial w}{\partial t}+\frac{\pi\bar{r}^3(r_o-r_i)}{s_{11}^{\mathrm{E}}}\frac{\partial^4 w}{\partial z^4}=\frac{\partial^2(M_{\mathrm{v}}\delta(z-L))}{\partial z^2} \tag{1}$$

with boundary conditions

$$\begin{gathered} w=0|_{z=0} \\ \frac{\partial w}{\partial z}=0|_{z=0} \\ m\frac{\partial^2 w}{\partial t^2}+c_{\mathrm{w}}\frac{\partial w}{\partial t}\,\mathrm{d}z=\frac{\pi\bar{r}^3(r_o-r_i)}{s_{11}^{\mathrm{E}}}\frac{\partial^3 w}{\partial z^3}\bigg|_{z=L} \\ \frac{\pi\bar{r}^3(r_o-r_i)}{s_{11}^{\mathrm{E}}}\frac{\partial^2 w}{\partial z^2}=0|_{z=L} \end{gathered} \tag{2}$$

where $w=w(z,t)$ denotes displacement in the x-direction, ρ is the piezotube density, A is the cross-sectional area of the piezotube, c_{w} is the damping coefficient, r_o and r_i are outer and inner radii of the piezotube, $\bar{r}=(r_o+r_i)/2$, s_{11}^{E} is the elastic compliance in the long-axis direction of the piezotube, $M_{\mathrm{v}}=(2\sqrt{2}\bar{r}^2 d_{31}V_x)/s_{11}^{\mathrm{E}}$ is a moment generated at the tip of the piezotube that affects the lateral dynamics, V_x is the applied voltage at the piezotube electrode, and d_{31} denotes a piezoelectric strain/charge coefficient.

Using the method of separation of variables by letting $w(z,t)=W(z)x(t)$, the lumped mass m_1, damping c_1, stiffness k_1, and actuator force F_{a} are obtained in the first mode, i.e.

$$\begin{gathered} m_1=\rho A\int_0^L W^2(z)\,\mathrm{d}z+mW^2(L) \\ c_1=c_{\mathrm{w}}\int_0^L W^2(z)\,\mathrm{d}z \\ k_1=\omega^2 m_1 \\ F_{\mathrm{a}}=\int_0^L W(z)\frac{\partial^2(M_{\mathrm{v}}\delta(z-L))}{\partial z^2}\,\mathrm{d}z \end{gathered} \tag{3}$$

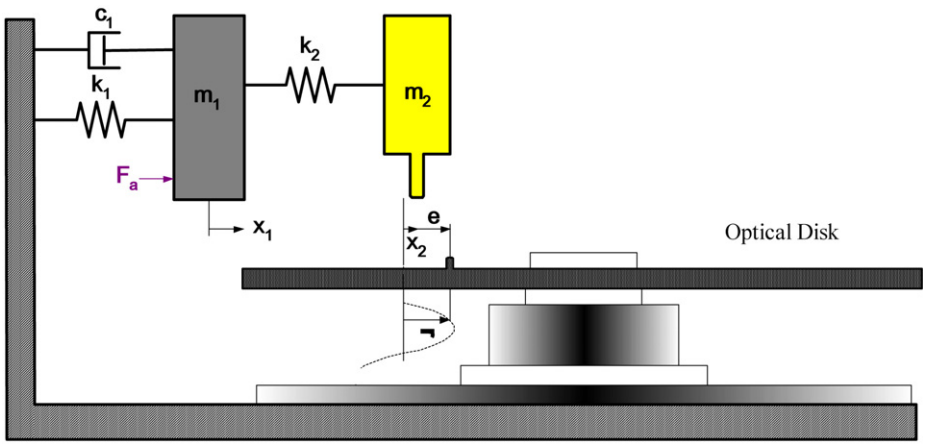

Figure 4. Tracking model in the presence of disk surface deformation.

where m is the sum of the cap B mass and a part of the suspension mass, i.e. $m = m_{cB} + 0.6m_s$. The first mode shape $W(z)$ of the lateral dynamics can be obtained from boundary conditions in equation (2) as [14]

$$W(z) = C_n\left\{(\cos pz - \cosh pz) + \frac{\cos pL + \cosh pL}{\sin pL + \sinh pL}(\sinh pz - \sin pz)\right\} \tag{4}$$

where C_n is arbitrary and $p = \sqrt[4]{[\rho A s_{11}^{E}\omega^2]/[\pi \bar{r}^3(r_o - r_i)]}$. ω is the first mode natural frequency to be obtained by solving the characteristic equation

$$pL(\cos pL\cosh pL + 1) + \frac{m}{\rho AL}(\cos pL\sinh pL - \cosh pL\sin pL) = 0. \tag{5}$$

Denoting a lumped mass m_2 as a part of the suspension mass and a pickup head mass, i.e. $m_2 = m_p + 0.4m_s$, where m_p denotes the pickup head mass, equations of motion according to figure 2 are written as

$$m_1\ddot{x}_1 = k_2(x_2 - x_1) - c_1\dot{x}_1 - k_1x_1 + F_a, \tag{6}$$

$$m_2\ddot{x}_2 = -k_2(x_2 - x_1), \tag{7}$$

where x_1 is the cap B displacement, x_2 is the pickup head displacement, and k_2 denotes the suspension stiffness.

3. Tracking motion in the presence of disk surface deformation

Figure 4 depicts a model for tracking motion in the presence of sinusoidal deformation of the disk surface. This study defines the tracking error as $e = r - x_2$, where r is the disk surface deformation. It is desired to minimize $e(t)$ to facilitate data reading/writing in near-field optical disk drives. Assume disk surface deformation r as a sinewave of frequency ω_a and amplitude A, i.e. $r = A\sin\omega_a t$. Therefore, the tracking error resulting from disk surface deformation is a sinewave of the same frequency but different amplitude and phase, i.e. $e_a = E_a\sin(\omega_a t - \theta_a)$. As a result, the displacement, velocity, and acceleration of the pickup head can be written as

$$\begin{aligned} x_2 &= r - e_a = A\sin\omega_a t - E_a\sin(\omega_a t - \theta_a)\\ \dot{x}_2 &= \dot{r} - \dot{e}_a = A\omega_a\cos\omega_a t - E_a\omega_a\cos(\omega_a t - \theta_a)\\ \ddot{x}_2 &= \ddot{r} - \ddot{e}_a = -A\omega_a^2\sin\omega_a t + E_a\omega_a^2\sin(\omega_a t - \theta_a). \end{aligned} \tag{8}$$

Substituting equation (8) into (7) yields

$$\begin{aligned} x_1 &= A\sin\omega_a t - E\sin(\omega_a t - \theta_a) + \frac{m_2}{k_2}\left[-A\omega_a^2\sin\omega_a t + E\omega_a^2\sin(\omega_a t - \theta_a)\right]\\ \dot{x}_1 &= A\omega_a\cos\omega_a t - E\omega_a\cos(\omega_a t - \theta_a) + \frac{m_2}{k_2}\left[-A\omega_a^3\cos\omega_a t + E\omega_a^3\cos(\omega_a t - \theta_a)\right]\\ \ddot{x}_1 &= -A\omega_a^2\sin\omega_a t + E\omega_a^2\sin(\omega_a t - \theta_a) + \frac{m_2}{k_2}\left[A\omega_a^4\sin\omega_a t - E\omega_a^4\sin(\omega_a t - \theta_a)\right]. \end{aligned} \tag{9}$$

This study describes a control force F_a based on the PD control method. Hence,

$$F_a = C_a\dot{e}_a + K_a e_a = C_a E_a\cos(\omega_a t - \theta_a) + K_a E_a\sin(\omega_a t - \theta_a) \tag{10}$$

where K_a is a proportional gain and C_a is a derivative gain. Substituting equations (8)–(10) into (6) yields

$$\frac{E_a}{A} = \left\{\left(\frac{m_1m_2}{k_2}\omega_a^4 - \left(m_2 + m_1 + \frac{k_1m_2}{k_2}\right)\omega_a^2 + k_1\right)\sin\omega_a t + \left(c_1\omega_a - \frac{c_1m_2}{k_2}\omega_a^3\right)\cos\omega_a t\right\}\left\{\left[\frac{m_1m_2}{k_2}\omega_a^4 - \left(m_2 + m_1 + \frac{k_1m_2}{k_2}\right)\omega_a^2 + (k_1 + K_a)\right]\sin(\omega_a t - \theta_a) + \left((c_1 + C_a)\omega_a - \frac{c_1m_2}{k_2}\omega_a^3\right)\cos(\omega_a t - \theta_a)\right\}^{-1}. \tag{11}$$

The ratio of amplitudes of E_a and A is thus written as

$$\frac{|E_a|}{|A|} = \left\{\left[\omega_a^4 - \left(\frac{k_1 + k_2}{m_1} + \frac{k_2}{m_2}\right)\omega_a^2 + \left(\frac{k_1}{m_1}\frac{k_2}{m_2}\right)\right]^2 + \left[\left(\frac{c_1}{m_1}\frac{k_2}{m_2}\right)\omega_a - \frac{c_1}{m_1}\omega_a^3\right]^2\right\}^{1/2}$$

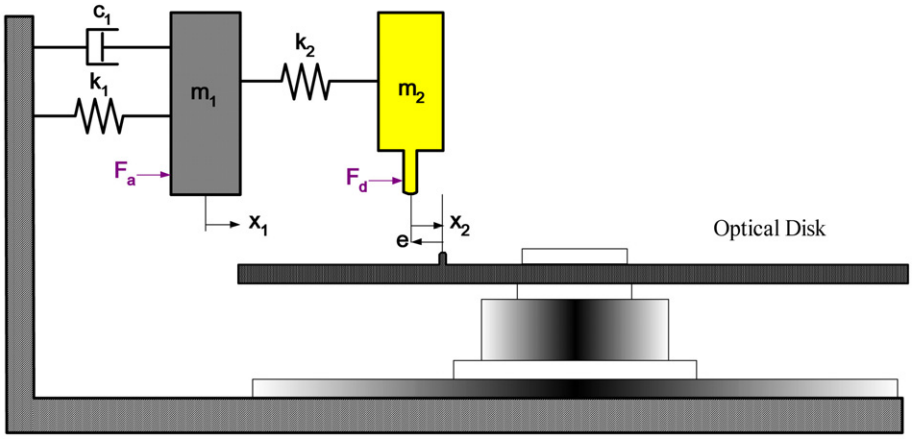

Figure 5. Tracking model in the presence of disturbance force.

$$\times\left\{\left\{\left[\omega_{\mathrm{a}}^4-\left(\frac{k_1+k_2}{m_1}+\frac{k_2}{m_2}\right)\omega_{\mathrm{a}}^2+\left(\frac{k_1+K_{\mathrm{a}}}{m_1}\frac{k_2}{m_2}\right)\right]^2+\left[\left(\frac{c_1+C_{\mathrm{a}}}{m_1}\frac{k_2}{m_2}\right)\omega_{\mathrm{a}}-\frac{c_1}{m_1}\omega_{\mathrm{a}}^3\right]^2\right\}^{1/2}\right\}^{-1}. \tag{12}$$

Corresponding to peak magnitudes in $|E_{\mathrm{a}}|/|A|$, letting the first term of the denominator in equation (12) be zero leads to roots

$$\begin{matrix}\omega_{\mathrm{r1}}^2\\ \omega_{\mathrm{r2}}^2\end{matrix}=\frac{1}{2}\left\{\left(\frac{k_1+k_2}{m_1}+\frac{k_2}{m_2}\right)\mp\sqrt{\left(\frac{k_1+k_2}{m_1}+\frac{k_2}{m_2}\right)^2-4\left(\frac{k_1+K_{\mathrm{a}}}{m_1}\frac{k_2}{m_2}\right)}\right\}. \tag{13}$$

If

$$\left(\frac{k_1+k_2}{m_1}+\frac{k_2}{m_2}\right)^2-4\left(\frac{k_1+K_{\mathrm{a}}}{m_1}\frac{k_2}{m_2}\right)>0, \tag{14}$$

i.e.

$$K_{\mathrm{a}}<\left(\frac{k_1+k_2}{m_1}+\frac{k_2}{m_2}\right)^2\frac{m_1m_2}{4k_2}-k_1, \tag{15}$$

then there are two resonant frequencies ω_{r1} and ω_{r2}. If

$$K_{\mathrm{a}}=K_{\mathrm{ac}}=\left(\frac{k_1+k_2}{m_1}+\frac{k_2}{m_2}\right)^2\frac{m_1m_2}{4k_2}-k_1 \tag{16}$$

then there are repeated roots, i.e. $\omega_{\mathrm{r1}}=\omega_{\mathrm{r2}}=\omega_r$, where K_{ac} and ω_r are called critical the proportional gain and critical resonant frequency, respectively. Moreover, if

$$K_{\mathrm{a}}>\left(\frac{k_1+k_2}{m_1}+\frac{k_2}{m_2}\right)^2\frac{m_1m_2}{4k_2}-k_1 \tag{17}$$

then the first term of the denominator in equation (12) is always positive, i.e. there is no resonance in the spectrum. From the first term of the numerator in equation (12), one obtains two anti-resonant frequencies, i.e.

$$\begin{matrix}\omega_{\mathrm{ar1}}\\ \omega_{\mathrm{ar2}}\end{matrix}=\sqrt{\frac{1}{2}\left\{\left(\frac{k_1+k_2}{m_1}+\frac{k_2}{m_2}\right)\mp\sqrt{\left(\frac{k_1+k_2}{m_1}+\frac{k_2}{m_2}\right)^2-4\left(\frac{k_1}{m_1}\cdot\frac{k_2}{m_2}\right)}\right\}}. \tag{18}$$

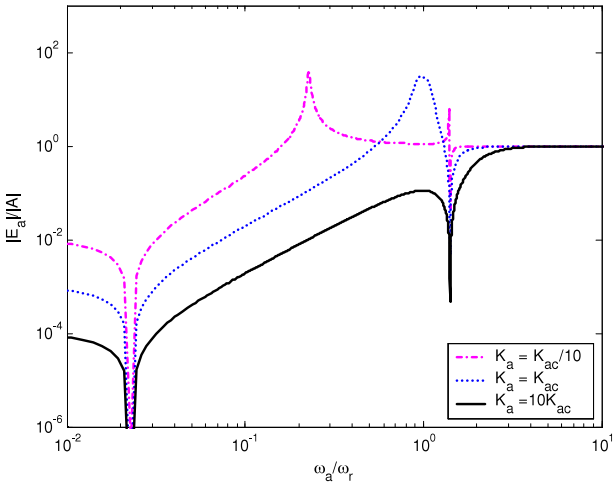

Figure 6. Effect of proportional gain K_{a} on the error ratio in the presence of sinusoidal deformation of the disk surface with $\zeta_{\mathrm{a}}=0.7$.

In the low-frequency region, i.e. $\omega_{\mathrm{a}}<\min(\omega_{\mathrm{r1}},\omega_{\mathrm{ar1}})$, it follows from equation (12) that the tracking error is expressed by

$$\frac{|E_{\mathrm{a}}|}{|A|}\approx\left(\frac{k_1}{k_1+K_{\mathrm{a}}}\right). \tag{19}$$

In the high-frequency region, i.e. $\omega_{\mathrm{a}}>\max(\omega_{\mathrm{r2}},\omega_{\mathrm{ar2}})$, the tracking error ratio is near one. If the disk surface deformation is expressed by a finite discrete Fourier series, i.e. $r(t)=\sum_{n=1}^{N}A_n\sin(n\omega_{0a}t-\theta_n)$, one can obtain the tracking error in the finite discrete Fourier series form, i.e. $e_{\mathrm{a}}(t)=\sum_{n=1}^{N}E_{na}\sin(n\omega_{0a}t-\theta_{na})$.

4. Tracking motion in the presence of disturbance force

Figure 5 depicts a model for tracking motion in the presence of a sinusoidal disturbance force. The equations of motion are written as

$$m_1\ddot{x}_1=k_2(x_2-x_1)-c_1\dot{x}_1-k_1x_1+F_{\mathrm{a}} \tag{20}$$

$$m_2\ddot{x}_2=-k_2(x_2-x_1)+F_{\mathrm{d}} \tag{21}$$

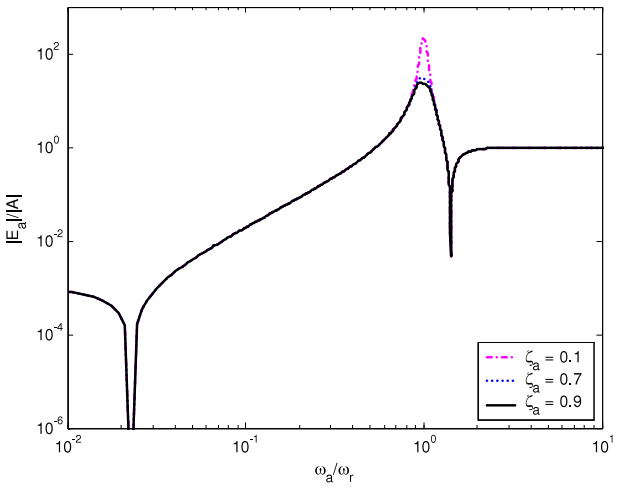

Figure 7. Effect of controller damping ζ_a on the error ratio in the presence of sinusoidal deformation of the disk surface with $K_a = K_{ac}$.

where $F_d = B \sin \omega t$ is a disturbance force acting on the pickup head. Assuming no disk surface deformation, i.e. $r = 0$, the tracking error resulting from the disturbance is a sinewave of the same frequency but with different amplitude and phase, i.e. $e_b = E_b \sin(\omega_b t - \theta_b)$. Hence,

$$\begin{aligned} x_2 &= r - e_b = -E_b \sin(\omega_b t - \theta_b) \\ \dot{x}_2 &= \dot{r} - \dot{e}_b = -E_b \omega_b \cos(\omega_b t - \theta_b) \\ \ddot{x}_2 &= \ddot{r} - \ddot{e}_b = E_b \omega_b^2 \sin(\omega_b t - \theta_b). \end{aligned} \tag{22}$$

Substituting equation (22) into equation (21) yields

$$\begin{aligned} x_1 &= -E_b \sin(\omega_b t - \theta_b) \\ &\quad + \frac{1}{k_2}[m_2 E_b \omega_b^2 \sin(\omega_b t - \theta_b) - B \sin \omega_b t] \\ \dot{x}_1 &= -E_b \omega_b \cos(\omega_b t - \theta_b) \\ &\quad + \frac{1}{k_2}[m_2 E_b \omega_b^3 \cos(\omega_b t - \theta_b) - B \omega_b \cos \omega_b t] \\ \ddot{x}_1 &= E_b \omega_b^2 \sin(\omega_b t - \theta_b) \\ &\quad + \frac{1}{k_2}[-m_2 E_b \omega_b^4 \sin(\omega_b t - \theta_b) + B \omega_b^2 \sin \omega_b t]. \end{aligned} \tag{23}$$

This study denotes F_a as a control force based on PD control; hence

$$\begin{aligned} F_a &= C_a \dot{e}_b + K_a e_b = C_a E_b \cos(\omega_b t - \theta_b) \\ &\quad + K_a E_b \sin(\omega_b t - \theta_b). \end{aligned} \tag{24}$$

Substituting equations (22)–(24) into equation (20) gives

$$\begin{aligned} \frac{E_b}{B} &= \left\{ \left(\frac{m_1}{k_2}\omega_b^2 - \frac{k_1}{k_2} - 1 \right) \sin \omega_b t + \left(-\frac{c_1}{k_2}\omega_b \right) \cos \omega_b t \right\} \\ &\quad \times \left\{ \left[\frac{m_1 m_2}{k_2}\omega_b^4 - \left(m_2 + m_1 + \frac{k_1 m_2}{k_2} \right) \omega_b^2 + (k_1 + K_a) \right] \right. \\ &\quad \times \sin(\omega_b t - \theta_b) + \left((c_1 + C_a)\,\omega_b - \frac{c_1 m_2}{k_2}\omega_b^3 \right) \\ &\quad \left. \times \cos(\omega_b t - \theta_b) \right\}^{-1}. \end{aligned} \tag{25}$$

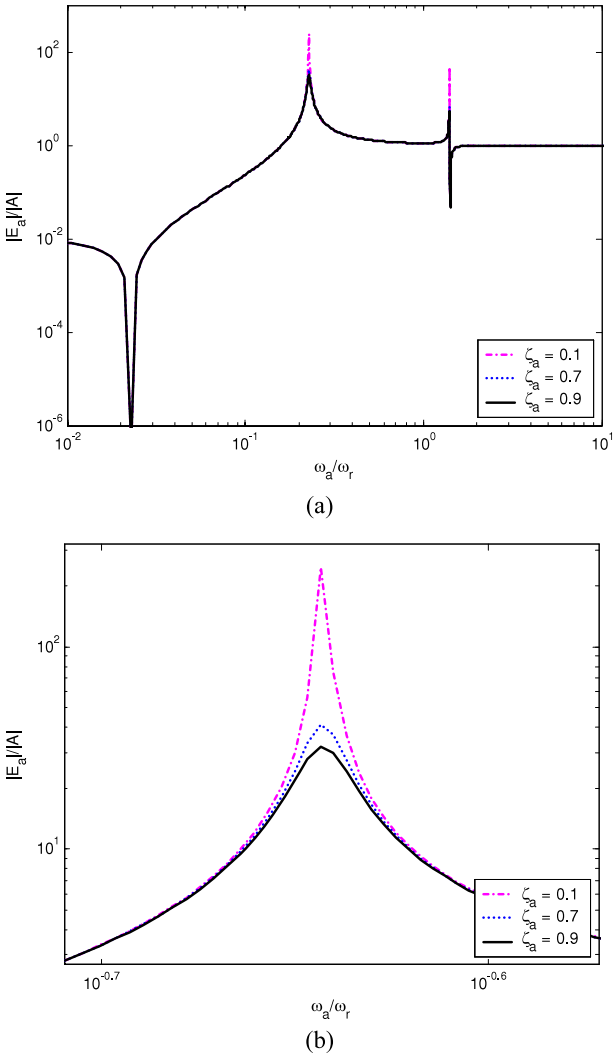

Figure 8. Effect of controller damping ζ_a on the error ratio in the presence of sinusoidal deformation of the disk surface with $K_a = K_{ac}/10$: (a) original spectrum, (b) detail of (a) near ω_{r1}.

Accordingly, the ratio of amplitudes of E_b and B is written as

$$\begin{aligned} \frac{|E_b|}{|B|} &= \left\{ \frac{1}{m_2} \sqrt{\left(\omega_b^2 - \frac{k_1 + k_2}{m_1} \right)^2 + \left(-\frac{c_1}{m_1}\omega_b \right)^2} \right\} \\ &\quad \times \left\{ \left\{ \left[\omega_b^4 - \left(\frac{k_1 + k_2}{m_1} + \frac{k_2}{m_2} \right) \omega_b^2 + \left(\frac{k_1 + K_a}{m_1} \frac{k_2}{m_2} \right) \right]^2 \right. \right. \\ &\quad \left. \left. + \left(\left(\frac{c_1 + C_a}{m_1} \frac{k_2}{m_2} \right) \omega_b - \frac{c_1}{m_1}\omega_b^3 \right)^2 \right\}^{1/2} \right\}^{-1}. \end{aligned} \tag{26}$$

The roots of the first term in the denominator of equation (26) are the same as those in equation (13). Accordingly, the resonant frequencies obtained from equation (26) are similar to equation (12). Dealing with the first term in the numerator of equation (26) leads to an anti-resonant frequency, i.e.

$$\omega_{ar} = \sqrt{\frac{k_1 + k_2}{m_1}}. \tag{27}$$

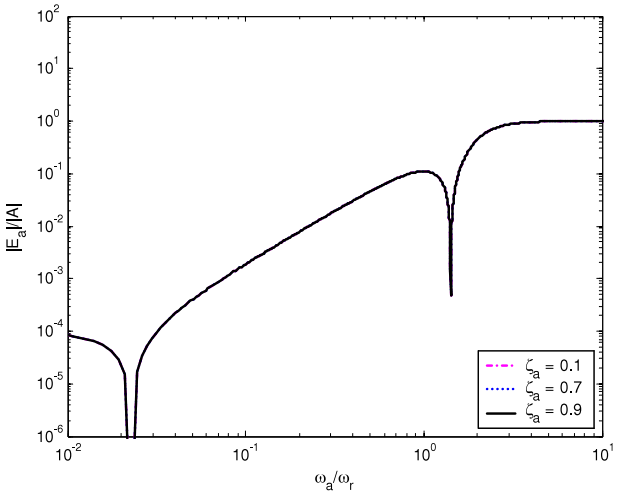

Figure 9. Effect of controller damping ζ_a on the error ratio in the presence of sinusoidal deformation of the disk surface with $K_a = 10K_{ac}$.

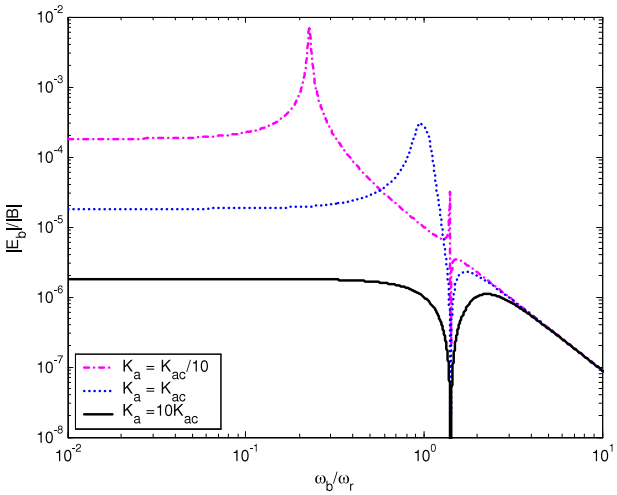

Figure 10. Effect of proportional gain K_a on the error ratio in the presence of a sinusoidal disturbance force with $\zeta_a = 0.7$.

Table 1. Parameters of the piezotube actuator.

m_{cB}	0.25×10^{-3} kg
m_s	0.175×10^{-3} kg
m_p	0.015×10^{-3} kg
d_{31}	-220×10^{-12} m V^{-1}
s_{11}^E	16.2×10^{-12} m^2 N^{-1}
ρ	7400 kg m^{-3}
c_w	0.01 kg s^{-1} m^{-1}
r_i	0.0025 m
r_o	0.003 175 m
k_2	56.71 N m^{-1}

In the low-frequency region, i.e. $\omega_b < \min(\omega_{r1}, \omega_{ar})$, based on equation (26), the tracking error is written as

$$\frac{|E_b|}{|B|} \approx \left(\frac{1}{k_1 + K_a}\right)\left(\frac{k_1 + k_2}{k_2}\right). \tag{28}$$

In the high-frequency region, i.e. $\omega_b > \max(\omega_{r2}, \omega_{ar})$, the tracking error ratio decreases with increasing ω_b^2. If the

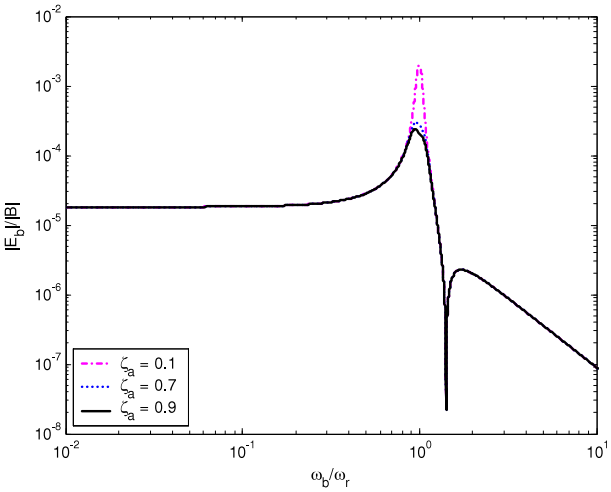

Figure 11. Effect of controller damping ζ_a on the error ratio in the presence of a sinusoidal disturbance force with $K_a = K_{ac}$.

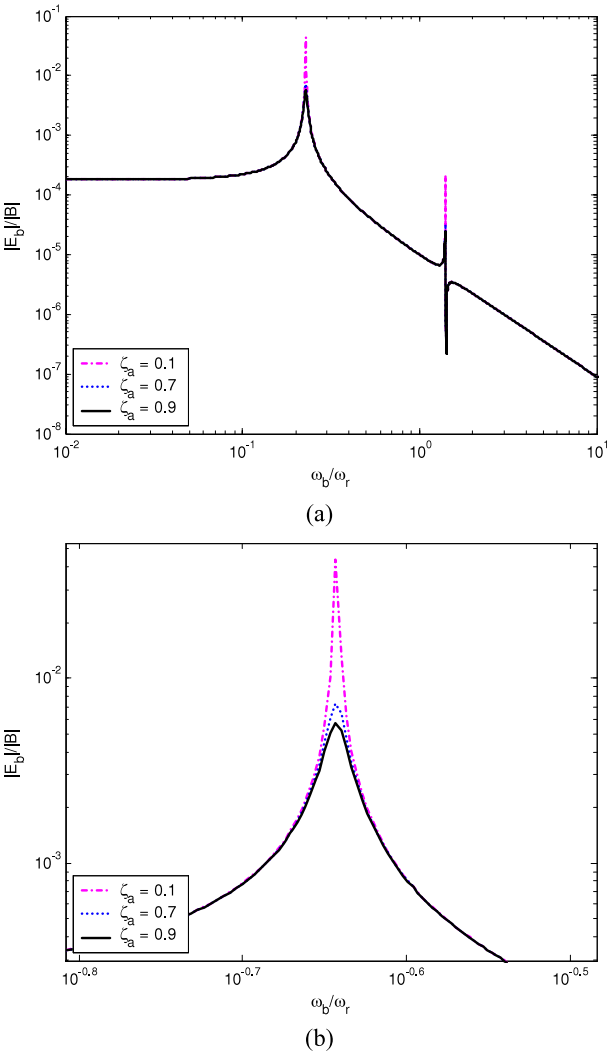

Figure 12. Effect of controller damping ζ_a on the error ratio in the presence of a sinusoidal disturbance force with $K_a = K_{ac}/10$: (a) original spectrum, (b) detail of (a) near ω_{r1}.

disturbance force is expressed by a finite discrete Fourier series, i.e. $F_d(t) = \sum_{n=1}^{N} B_n \sin(n\omega_{0b}t - \theta_{nb})$, one can

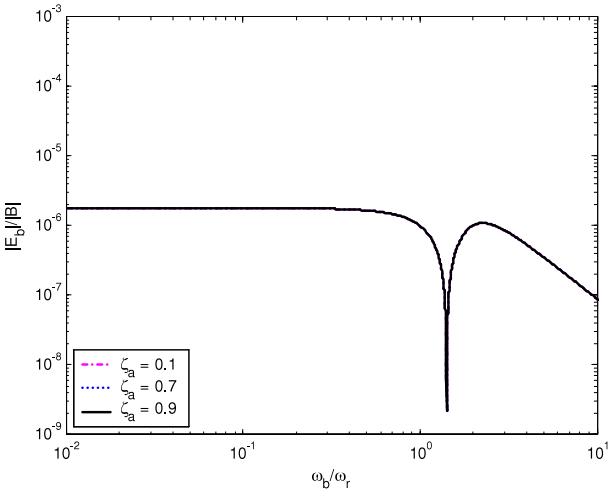

Figure 13. Effect of controller damping ζ_a on the error ratio in the presence of a sinusoidal disturbance force with $K_a = 10K_{ac}$.

obtain the tracking error in finite discrete Fourier series form, i.e. $e_b(t) = \sum_{n=1}^{N} E_{nb} \sin(n\omega_{0b}t - \theta_{nb})$.

5. Numerical result

To carry out numerical simulation based on the previous theoretical derivation, the piezotube length is prescribed as 19.0 mm. Assuming the parameters listed in table 1, spectrum results of the error ratio in the presence of disk surface deformation are obtained by calculating equation (12) with $L = 19.0$ mm. The error ratio $|E_a|/|A|$ varies with the frequency ratio and the proportional gain K_a as shown in figure 6, where $\zeta_a = C_a/[2\sqrt{K_a(m_1 + m_2)}]$ denotes controller damping. The error ratio curves show two anti-resonances. A larger K_a (at $K_a > K_{ac}$) results in less tracking error and no resonance; i.e. the error ratio is always smaller than one. The variation of error ratios with the frequency ratio and the damping ratio ζ_a at $K_a = K_{ac}$, $K_a = K_{ac}/10$ and $K_a = 10K_{ac}$ are shown in figures 7–9, respectively. A larger ζ_a generates less tracking error at $K_a = K_{ac}$ and $K_a = K_{ac}/10$, but ζ_a does not affect the error at $K_a = 10K_{ac}$ since the three curves coincide in figure 9. Furthermore, calculating equation (26) yields spectrum results of error ratios in the presence of a disturbance force. The error ratio $|E_b|/|B|$ varies with the frequency ratio and the proportional gain K_a as shown in figure 10, where larger K_a results in less tracking error and no resonance. Figures 11–13 depict the error ratio varying with the frequency ratio and damping ratio ζ_a at $K_a = K_{ac}$, $K_a = K_{ac}/10$ and $K_a = 10K_{ac}$. Accordingly, a larger ζ_a decreases the error ratio more at $K_a = K_{ac}$ and $K_a = K_{ac}/10$, but ζ_a does not influence the error ratio at $K_a = 10K_{ac}$, since the three curves coincide in figure 13.

6. Conclusion

Based on tracking the motion spectrum, this study has investigated motion error during track-following and focusing for pickup heads in the presence of disk surface deformation and disturbance force with a piezotube actuator installed in the pickup head. In the tracking motion analysis applying PD control, there exists a critical proportional gain calculated from the piezotube and suspension assembly parameters. There is only one resonance or none in the frequency spectra when the proportional gain is larger than the critical proportional gain. No resonance implies that the tracking error ratio is smaller than one, which is demonstrated in figures 9 and 13. Moreover, the critical proportional gain is found to be more important than the controller damping.

Acknowledgment

The authors gratefully acknowledge the support of the 'Pursuing Academic Excellence Project' by the National Science Council in Taiwan, ROC under grant no. NSC94-2752-E009-009-PAE.

References

[1] Mizuno T, Kojima N, Hitosugi T, Sako K and Watanase K 2004 An optical configuration based on flying head structure for near-field recording *Japan. J. Appl. Phys.* **43** 1403–9

[2] Zijp F, van der Mark M, Verschuren C, Lee J, van den Eerenbeemd J, Urbach P and van der Aa M 2005 High-density near-field optical recording with a solid immersion lens, conventional actuator and a robust air gap servo *IEEE Trans. Mag.* **41** 1042–6

[3] Saito K, Ishimoto T, Kondo T, Nakaoki A, Masuhara S, Furuki M and Yamamoto M 2002 Readout method for read only memory signal and air gap control signal in a near field optical disc system *Japan. J. Appl. Phys.* **41** 1898–902

[4] Kim S, Kim Y, Park J M, Kim J Y and Kim J H 2002 Effective design and performance of an optical flying head for near-field recording *Japan. J. Appl. Phys.* **41** 1884–8

[5] Wu W C and Liu T S 2005 Frequency-shaped sliding mode control for flying height of pickup head in near-field optical disk drives *IEEE Trans. Mag.* **41** 1061–3

[6] Taylor M E 1993 Dynamics of piezoelectric tube scanners for scanning probe microscopy *Rev. Sci. Instrum.* **64** 154–8

[7] Ohara T and Youcef-Toumi K 1995 Dynamics and control of piezotube actuators for subnanometer precision applications *Proc. Conf. on American Control (Seattle, WA)* pp 3808–12

[8] Tanaka H, Kohira H and Matsumoto M 2001 Effect of air-bearing design on slider dynamics during unloading process *IEEE Trans. Mag.* **37** 1818–20

[9] Kim S, Han G and Son H 1998 Dynamic characteristics of disk vibration and rotating airflow in magneto optical drive *IEEE Int. Conf. on Consumer Electronics (Los Angeles, CA)* pp 106–8

[10] Honchi M, Kohira H and Matsumoto M 2003 Numerical simulation of slider dynamics during slider-disk contact *Tribol. Int.* **36** 235–40

[11] Kim S, Park J, Park G, Lee J, Lee J and Jung H 2004 An optical flying head assembly for a small-form-factor plastic disk in PCMCIA-like drive *Japan. J. Appl. Phys.* **43** 4752–8

[12] Hong E, Oh W S, Park N C, Yang H S and Park Y P 2004 Dynamic shock analysis of the head-disk assembly for small form factor optical disk drives *Conf. on Asia-Pacific Data Storage (Taoyuan, Taiwan)* pp 84–5

[13] Kim S, Yoon S J, Choi D H and Lee S Y 2005 A study on the flying stability of optical flying head on the plastic disks *IEEE Trans. Mag.* **41** 986–8

[14] Clough R W and Penzien J 1993 *Dynamics of Structures* (New York: McGraw-Hill)